



**HAL**  
open science

## Collision-induced hyper-Rayleigh light scattering in gaseous dihydrogen-neon mixtures

Waldemar Glaz, Jean-Luc Godet, Anastasios Haskopoulos, Tadeusz Bancewicz, George Maroulis

► **To cite this version:**

Waldemar Glaz, Jean-Luc Godet, Anastasios Haskopoulos, Tadeusz Bancewicz, George Maroulis. Collision-induced hyper-Rayleigh light scattering in gaseous dihydrogen-neon mixtures. *Physical Review A*, 2011, 84 (1), pp.012503. 10.1103/PhysRevA.84.012503 . hal-03187582

**HAL Id: hal-03187582**

**<https://univ-angers.hal.science/hal-03187582>**

Submitted on 24 May 2021

**HAL** is a multi-disciplinary open access archive for the deposit and dissemination of scientific research documents, whether they are published or not. The documents may come from teaching and research institutions in France or abroad, or from public or private research centers.

L'archive ouverte pluridisciplinaire **HAL**, est destinée au dépôt et à la diffusion de documents scientifiques de niveau recherche, publiés ou non, émanant des établissements d'enseignement et de recherche français ou étrangers, des laboratoires publics ou privés.

# Collision-induced hyper-Rayleigh light scattering in gaseous dihydrogen-neon mixtures

W. Głaz,<sup>1</sup> J.-L. Godet,<sup>2</sup> A. Haskopoulos,<sup>3</sup> T. Bancewicz,<sup>1,\*</sup> and G. Maroulis<sup>3,†</sup>

<sup>1</sup>*Nonlinear Optics Division, Faculty of Physics, Adam Mickiewicz University, Umultowska 85, PL-61-614 Poznań, Poland*

<sup>2</sup>*Laboratoire de Photonique d'Angers, EA 4464, Université d'Angers, 2 boulevard Lavoisier, F-49045 Angers Cedex 01, France*

<sup>3</sup>*Department of Chemistry, University of Patras, GR-26500 Patras, Greece*

(Received 10 February 2011; revised manuscript received 14 May 2011; published 11 July 2011)

Cartesian components of the collision-induced (CI) hyperpolarizability  $\Delta\beta$  tensor are computed for the linear, T-shaped, and  $45^\circ$  configurations of the  $\text{H}_2$ -Ne pair in the intermolecular range 3 to 14 bohr. Symmetry-adapted components  $\Delta\beta_{\lambda L}^{(K)}(R)$  of the vector ( $K = 1$ ) part, as well as the septor ( $K = 3$ ) part, of the  $\text{H}_2$ -Ne CI hyperpolarizability are calculated starting from the *ab initio* Cartesian hyperpolarizability tensor values transformed into their spherical counterparts. By applying these quantities, the vector together with the septor collision-induced hyper-Rayleigh (CIHR) spectra for the  $\text{H}_2$ -Ne binary gas mixture are determined in the frequency range from  $-1250$  to  $2500 \text{ cm}^{-1}$ . The profiles are partially employed as a benchmarking device to estimate the importance of the short intermolecular distance part of the  $\Delta\beta(R)$  dependence. The depolarization ratio of the CIHR spectra in the whole frequency range is also calculated. The nature of the CIHR signal and the feasibility of the related experiments are discussed and analyzed.

DOI: [10.1103/PhysRevA.84.012503](https://doi.org/10.1103/PhysRevA.84.012503)

PACS number(s): 33.70.-w, 33.20.Fb, 33.80.Gj

## I. INTRODUCTION

Many years ago, dihydrogen was recognized as a system of primary importance to molecular astrophysics [1,2]. Intermolecular interactions involving dihydrogen have been extensively studied. Collision-induced absorption by dihydrogen pairs has attracted considerable attention [3]. Additional interest in the interaction of dihydrogen with other molecular systems stems from the fact that physisorption is one of the methods that could be of use for hydrogen-storage technologies [4,5]. Dihydrogen interacting with rare-gas atoms ( $\text{H}_2$ -Rg) and related spectra has been systematically studied [6]. This has attracted even more attention recently [7] as it is relevant to experimental efforts to produce ultracold  $\text{H}_2$  [8]. In this paper we focus on the  $\text{H}_2$ -Ne pair, a system of current experimental [9] and theoretical interest [10]. Our aim is to predict theoretical collision-induced hyper-Rayleigh (HR) spectra for the gas-phase dihydrogen-neon system. Details of the calculations we have carried out in the work are reported in Sec. III; the method for calculating the symmetry-adapted (SA) components of the hyperpolarizability is presented there together with a description of the fitting procedure used. In Sec. III D the two main methods of evaluating the profiles—semiclassical (SC) and quantum mechanical (QM)—are outlined. The CIHR intensities are given in absolute units. We also consider the feasibility of the CIHR experiment in Sec. II and in the Discussion. In the latter part of the work we deliberate on the possibility of extracting the values of the spectral moments associated with various symmetry-adapted components of the first hyperpolarizability tensor from experimental profiles. The final section is devoted to analyzing the spectral properties obtained, especially their behavior determined by the  $\Delta\beta(\mathbf{R})$  dependence within different intermolecular separation regions.

## II. EXPERIMENTAL REMARKS

The rationale of studying the collisional hyper-Rayleigh effect is mainly determined by the expected capability of effective measurements of the phenomenon. In this respect, the computed CIHR absolute intensities can provide crucial information. In the HR experiments reported in Ref. [11], Pyatt and Shelton were able to detect signals higher than  $\approx 2 \times 10^{-4}$  cps for a spectral slit width of  $25 \text{ cm}^{-1}$ , i.e.,  $\approx 8 \times 10^{-6}$  cps  $\text{cm}^{-1}$ . Let us consider this experimental threshold as a reference and consider a pulsed laser, for instance one of the Nd:YAG (yttrium aluminum garnet) family devices, whose beam has a Gaussian profile. The parameters of the beam at the focus are the energy of its pulse  $\epsilon_L$ , repetition rate  $r$ , pulse duration  $\tau$ , beam waist  $w_0$ , and Rayleigh length  $z_R = \pi w_0^2 / \lambda_L$ , where  $\lambda_L$  is the wavelength of the laser. The HR scattering volume can be approximately considered as equal to  $V_s = 2z_R \pi w_0^2$  whereas the maximum irradiance at the focus,  $\mathfrak{S}_0$ , can be expressed as [12]

$$\mathfrak{S}_0 = \frac{4\epsilon_L \sqrt{\pi \ln 2}}{\tau} \left( \frac{1}{\pi w_0} \right)^2. \quad (1)$$

Moreover, the energy scattered per second,  $E_s$ , is proportional to  $\mathfrak{S}_0^2 V_s$ , the solid collection angle  $\Omega_s$ , the total duration per second of the illumination  $r\tau$ , the density numbers of the gases ( $n_{\text{H}_2}$  and  $n_{\text{Rg}}$ ), and the CIHR intensity  $I(\nu)$ :

$$E_s = \Omega_s V_s n_{\text{H}_2} n_{\text{Rg}} r \tau \mathfrak{S}_0^2 I(\nu). \quad (2)$$

Dividing this energy by the energy of the scattered photon ( $2hc/\lambda_L$ ), we get the corresponding number of cps  $\text{cm}^{-1}$ ,

$$N = 1.3 \times 10^{69} \Omega_s n_{\text{H}_2}^* n_{\text{Rg}}^* \frac{r \epsilon_L^2}{\tau} I(\nu), \quad (3)$$

where the number densities  $n_\chi^*$ , the energy of the pulse, and the CIHR intensity  $I(\nu)$  are expressed in amagats, joules, and  $\text{cm}^8 \text{ s erg}^{-1}$ , respectively. Typically,  $\Omega_s \approx 0.1$  sr. To obtain a high signal, only the density numbers and the laser characteristics can be changed. Taking for example  $n_\chi^* \approx 50$  amagat and a high-repetition-rate picosynchronous

\*tbancewi@zon12.physd.amu.edu.pl

†maroulis@upatras.gr

Nd:YAG laser characterized by  $\epsilon_L = 0.3$  mJ,  $r = 6$  kHz, and  $\tau = 200$  ps [13], we can show from Eq. (3) that  $N > 8 \times 10^{-6}$  cm s $^{-1}$  if  $I(\nu) > 10^{-83}$  cm $^8$  s erg $^{-1}$ . Indeed, light losses due to the experimental optical setup can be important and, at least, we must consider the upper order of magnitude to be  $10^{-82}$  cm $^8$  s erg $^{-1}$ . However, this shows that the HR spectra recently studied by our group in a purely theoretical way could be scanned experimentally in a wide frequency range relative to the central frequency  $2\nu_L$  [14–17]. This would offer the possibility of extracting from the spectra crucial information about the symmetry-adapted components, as we will see further in the case here considered, H $_2$ -Ne.

### III. SPECTRAL CALCULATIONS

The blueprint for the presented study has four major steps following the footprints of our previous works: quantum chemistry (QC) *ab initio* calculations of the hyperpolarizability properties of the compound considered, evaluation of the symmetry-adapted components of the hyperpolarizability tensor and their fitted dependencies on the intermolecular distance  $R$ , translational spectral contribution computations, and finally, determination of the resulting full rototranslational lines of CIHR spectra [14–19].

#### A. *Ab initio* computations

We assume that the H $_2$ -Ne system is fixed in the  $xz$  plane with the atom on the positive side of  $z$ . We compute the hyperpolarizability tensors for the H $_2$ -Ne pair as a function of their relative separation  $R$  and for the orientations of  $0^\circ$ ,  $45^\circ$ , and  $90^\circ$  between the relative intermolecular vector  $\mathbf{R}$  pointing from the center of mass of H $_2$  to the center of Ne and the H-H bond. In our computations we assume that  $r_{\text{H-H}} = 1.449a_0$  [20].

The interaction electric properties of the supermolecules are obtained via the well-tested Boys-Bernardi counterpoise-correction (CP) method [21]. The interaction quantity  $P_{\text{int}}(\text{H}_2 \cdots \text{Ne})(\mathbf{R})$  at a given internuclear separation  $\mathbf{R}$  is computed as

$$P_{\text{int}}(\text{H}_2 \cdots \text{Ne})(\mathbf{R}) = P(\text{H}_2 \cdots \text{Ne})(\mathbf{R}) - P(\text{H}_2 \cdots \text{X})(\mathbf{R}) - P(\text{X} \cdots \text{Ne})(\mathbf{R}).$$

All calculations were performed at the coupled-cluster with singles and doubles (CCSD) level of theory with the GAUSSIAN03 program [22]. All electrons were correlated. Full descriptions of the CCSD method are readily available in standard textbooks [23]. To a large extent, the successful calculation of interaction-induced electric properties depends on the selection of suitable basis sets. In this work we chose the basis set [6s4p3d] for H and [7s5p4d1f] for Ne. The H part of this basis is an augmented version of the [6s4p1d] purpose-oriented molecule specific basis set used previously in the calculations of the interaction-induced (hyper)polarizability of H $_2$ -H $_2$  [24] and the [6s4p2d] basis used for the H $_2$ -Ar pair [25]. The  $d$ -GTF (Gaussian-type functions) exponents of the [6s4p3d] basis for H are  $\eta_d = 0.8984a_0^{-2}$ ,  $0.1246a_0^{-2}$ , and  $0.0464a_0^{-2}$ . The [6s4p3d] basis set yields a self-consistent field (SCF) polarizability of  $5.4607e^2a_0^2E_h^{-1}$ , compared with

$5.4605e^2a_0^2E_h^{-1}$  obtained with the [6s4p2d] basis [25]. The [7s5p4d1f] basis set used for Ne, well-tested in interaction-induced electric property calculations on Ne-Ne, is taken from previous work [24]. At the SCF level of theory it gives for the Ne dipole polarizability the value of  $\alpha/e^2a_0^2E_h^{-1} = 2.3719$ , compared to the numerical Hartree-Fock (NHF) [26] value of 2.37674.

To check the stability of the hyperpolarizability values we performed further tests with even larger basis sets. Thus, since  $A = [6s4p3d/7s5p4d1f]$  is the basis set used in this work, we performed additional calculations with basis sets  $B = [6s4p3d/9s6p5d1f]$  and  $C = [6s4p3d1f/9s6p5d1f]$ . We chose the linear configuration of H $_2$ -Ne with Ne placed at a distance of  $4.0a_0$  from the midpoint of the dihydrogen. We expect this choice to be particularly advantageous for a severe test of basis-set effects. We obtained the following interaction-induced hyperpolarizability values at the CCSD (full) level of theory:  $\Delta\beta_{zzz} = 16.67$  (basis A), 16.65 (basis B), and 16.64 (basis C). This remarkable stability is also present in calculations on the T-shaped system, at the same separation. Relying on the above observation, we are led to accept an uncertainty for our hyperpolarizability values as significantly better than 2.0% in all cases. According to our assessment, this accuracy level is the main factor shaping the quality of results at the further stages of our spectral calculations.

A full presentation of the computational approach, including basis-set effects on the calculated properties and the relative merit of the *ab initio* methods, will be given elsewhere [27]. Computed Cartesian components of the CI H $_2$ -Ne hyperpolarizability tensor are available from the corresponding authors upon request.

#### B. Computation of the symmetry-adapted components

We will write the sets of equations for the symmetry-adapted collision-induced hyperpolarizability components  $\Delta\beta_{\lambda L}^{(K)}(R)$ , see Refs. [18,19]. Next, by using the advanced QC methods described in Sec. III A we compute the Cartesian components of the first hyperpolarizability tensor of H $_2$ -Ne for three intermolecular configurations—the linear, L-shaped symmetry, the  $45^\circ$  configuration and the T-symmetry shape; all components are computed for the intermolecular range  $R$  from 3 to 14 bohr. The first step in calculating the symmetry-adapted components  $\Delta\beta_{\lambda L}^{(K)}(R)$  of the H $_2$ -Ne first-hyperpolarizability tensor  $\Delta\beta$  requires a transformation of Cartesian hyperpolarizability components to spherical irreducible ones. The coefficients of this transformation are discussed, for instance, in Refs. [18,28]. There are certain restrictions imposed upon the symmetry-adapted coefficients  $\Delta\beta_{\lambda L}^{(K)}(R)$  by the geometry of the system. We have discussed them in our previous studies [18,19]. Let us also note that we obtain a separate set of equations for the vector  $\Delta\beta_{\lambda L}^{(1)}(R)$  SA components and another set for the septor  $\Delta\beta_{\lambda L}^{(3)}(R)$  SA components. The symmetry-adapted components of the vector part of the CI hyperpolarizability tensor are presented in Fig. 1, whereas the components of the septor part are given in Fig. 2.

#### C. Fitting functions

The numerical *ab initio* discrete data sets, both those determining the potential surface as well as the

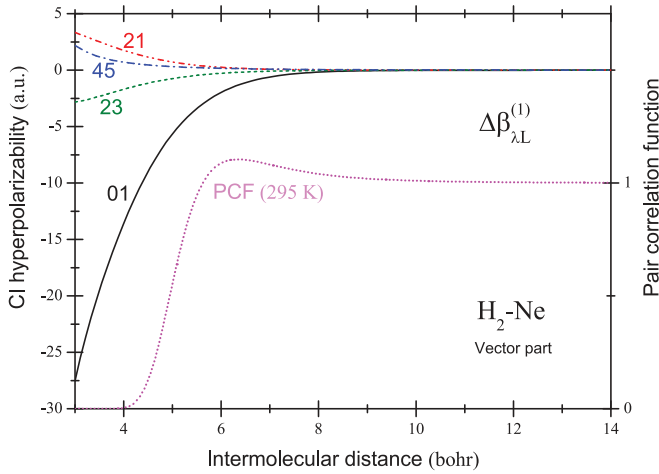


FIG. 1. (Color online) The  $R$  dependence of the  $\Delta\beta_{\lambda L}^{(1)}(R)$  irreducible spherical rotationally adapted component of the vector part of the CI first dipole hyperpolarizability tensor for  $\text{H}_2\text{-Ne}$  expressed in atomic units. Curves are labeled by  $\lambda L$ . In addition, we present the shape of the semiclassical pair correlation function (PCF) at 295 K for the intermolecular potential given in Ref. [10]; a discussion of the result uncertainties is within the text (Secs. III A, III C, and IV A).

hyperpolarizability dependence on the intermolecular distance, were used in the form of a continuous function obtained by means of the nonlinear least square Marquardt-Levenberg method [29]. The potential can be satisfactorily estimated by a series expansion of the form

$$V(R) = (q_0 R^2 + q_1 R + q_2) \exp(q_3 R + q_4) - \frac{|q_5|}{R^6} + \sum_{i=7}^{22} \frac{q_{i-1}}{R^i}, \quad (4)$$

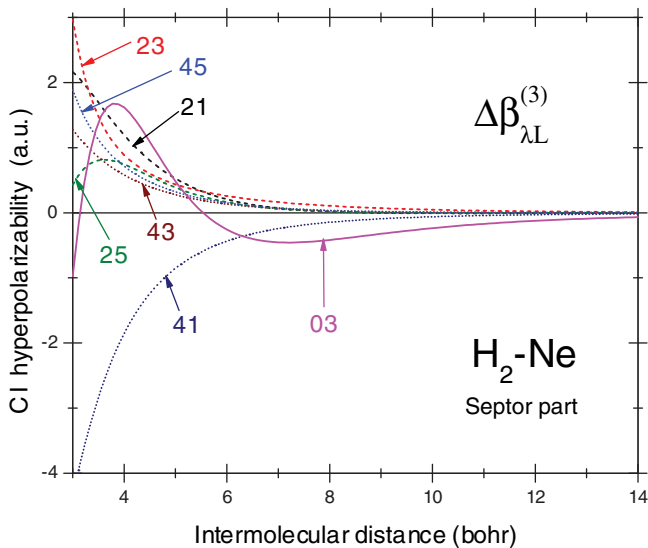


FIG. 2. (Color online) The  $R$  dependence of the  $\Delta\beta_{\lambda L}^{(3)}(R)$  irreducible spherical rotationally adapted component of the septor part of the CI first dipole hyperpolarizability tensor for  $\text{H}_2\text{-Ne}$  given in atomic units. Curves are labeled by  $\lambda L$ ; a discussion of the result uncertainties is within the text (Secs. III A, III C, and IV A).

where the first term represents a short-range effect related to *exchange* or *overlap* type interactions [30,31], whereas the second part of the formula, distinguished from the series expansion, is introduced to enable the long-range part of the potential to diminish according to a  $\sim 1/R^6$  dependence; the other far-distance contributions (including dispersion- and induction-like processes) are entangled in the final summation. The  $q_i$  parameters are obtained by fitting the function to the *ab initio* data sets reported in Ref. [10]. The discrepancy between the fit and the QC values does not exceed 0.015% of the relative root mean square deviation (RRMSD), which proves the high accuracy of the potential function used, especially in view of the *very good* agreement between the original QC data set and the experiment claimed in Ref. [10].

The symmetry-adapted hyperpolarizability components' dependence on  $R$  is also modeled by applying the following analytical formula:

$$\Delta\beta_{\lambda L}^{(K)}(R) = (A_1 R^2 + A_2 R + A_3) \exp(A_4 R + A_5 R^2) + \frac{B_1}{R^4} + \frac{B_2}{R^6} + \sum_{i=1}^4 \frac{C_i}{R^{2n+5}}, \quad (5)$$

where the exponential part of the function reflects the exchange and overlap interaction influences, while the presence of the multipolar effects,  $\sim 1/R^4$  and  $\sim 1/R^6$  [31,32], is emphasized by singling them out of the long-range expansion series, separate from the third section of the expression, for which dispersion forces are mainly responsible. The  $A_i$ ,  $B_i$ , and  $C_i$  coefficients represent fitting parameters of the hyperpolarizability symmetry-adapted components. The quality of the functions fitted can be estimated by comparing their values with the original QC data sets. As a result we obtain a percentage deviation ranging from a tiny fraction of per cent to  $\sim 3.0\%$  with the RRMSD reaching  $\sim 2.0\%$  for the intermolecular distances of interest. In Fig. 1 we plot the fitted lines for the vector SA contributions, whereas those for the septor part are given in Fig. 2. The fitting coefficients are available from the corresponding authors upon request.

#### D. Rotational, translational, and convoluted CIHR spectra

As far as the molecular pair  $\text{H}_2\text{-Ne}$  is concerned, each constituent monomer of it is spherical or may be treated as quasispherical; therefore, the intermolecular potential can, consequently, be regarded as isotropic. Hence, the translational and rotational motions become separable and the CIHR intensities associated with the vector and septor parts of the hyperpolarizability tensor can be written as a series of convolution products [33]:

$$I^{(K)}(\omega) = \frac{\pi}{2c} k_s^4 \sum_{\lambda L} d_\lambda(\omega) * g_{\lambda L}^{(K)}(\omega), \quad (6)$$

where  $k_s$  is the wave vector of the scattered light,  $g_{\lambda L}^{(K)}(\omega)$  is the translational function (TRF) associated with the symmetry-adapted component  $\Delta\beta_{\lambda L}^{(K)}(R)$ , and  $d_\lambda(\omega)$  stands for the rotational stick spectrum (RSS) related to a given value of  $\lambda$  (for more details, see Ref. [33]). The RSS is normalized to 1 and the TRF are at the origin of the absolute intensities of the CIHR spectra. In order to calculate these TRF, we use the intermolecular potential recently provided by Lique [10].

Moreover, we apply two methods of calculation of the translational spectra associated with the symmetry-adapted components of the hyperpolarizability tensor—the quantum-mechanical and the semiclassical methods. The QM and SC approaches are presented in detail in many papers devoted for instance to the CIHR spectra of H<sub>2</sub>-Ar [33] and H<sub>2</sub>-He [19].

The basic quantities shaping the collisional translational spectra within the QM model are squared matrix elements of the radial-dependent symmetry-adapted components of the intermolecular hyperpolarizabilities:

$$\begin{aligned} & |(\Delta\beta_{\lambda L}^{(K)})'_l(E, \omega)|^2 \\ &= \left| \int_0^\infty \hat{\Psi}^*(R; E', l') \Delta\beta_{\lambda L}^{(K)}(R) \hat{\Psi}(R; E, l) dR \right|^2, \\ & E' = E + \hbar\omega. \end{aligned} \quad (7)$$

In the expression above the radial wave functions  $\Psi(R; E, l)/R$  are solutions of the Schrödinger equation for the relative translational motion of H<sub>2</sub> and Ne [30]. The quantum numerical procedure used to evaluate these matrix elements was designed with respect to state-of-the-art requirements and tested on model systems for which analytical results could have been calculated, with an accuracy established varying between 0.006% and 1.3% [34]. A more complete description of the details of the quantum numerical method can be found in Refs. [34–36] and in the papers cited therein. In the SC case the molecular trajectories are computed in terms of functions dependent on velocities and collisional parameters. Subsequently the Fourier transforms of the hyperpolarizability components  $\Delta\beta_{\lambda L}^{(K)}(R)$  are determined according to the formulas established by Posch [37] and the resulting classical spectra are desymmetrized by taking into account the *sum rules* values of the semiclassical moments  $M_0$ ,  $M_1$ , and  $M_2$  [33].

#### IV. RESULTS AND DISCUSSION

The results obtained and discussed below in more detail make a natural basis for determination of the values of the supermolecular nonlinear properties by experimental methods when available. They also provide an opportunity to study the importance of specific collision mechanisms generating the first hyperpolarizability. The research into the  $\Delta\beta(R)$  dependence is also a valuable tool for the assessment of what intermolecular separation range is to be taken into account in calculations related to nonlinear light-scattering processes.

##### A. CIHR theoretical spectra

The theoretical spectra  $I^{(K)}$  associated with the vector and septor parts of the hyperpolarizability tensor were obtained from Eq. (6). They are given in absolute units ( $\text{cm}^8 \text{ s erg}^{-1}$ ) in Figs. 3 and 4, which also present the spectral lines for  $\lambda = 0, 2, 4$ . The high accuracy of the numerical algorithms that was mentioned in the previous sections means that the resulting spectra are, in general, as good as the underlying QC *ab initio* hyperpolarizability values, so that the uncertainties expected should be of order not exceeding 5.0%—the commonly acceptable limit in experimental studies [30]. The calculated QM and SC translational profiles are generally close to each

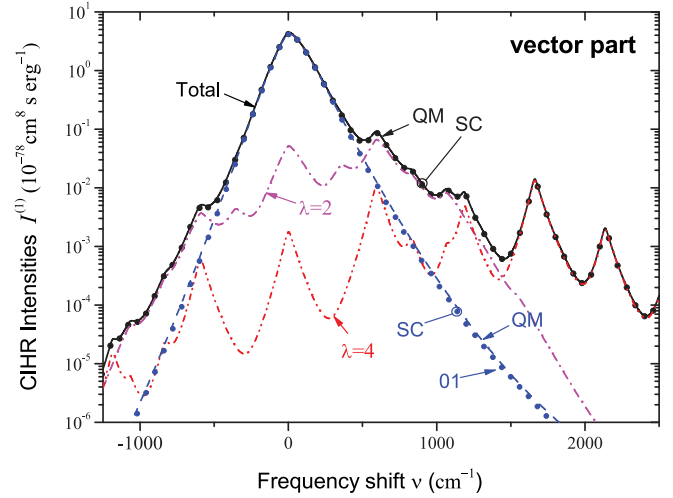


FIG. 3. (Color online) The CIHR binary polarized vector spectrum  $I_{\perp}$  (in  $\text{cm}^8 \text{ s erg}^{-1}$ ) of the H<sub>2</sub>-Ne pair at  $T = 295 \text{ K}$ , versus frequency shift ( $\nu$ , in  $\text{cm}^{-1}$ ) with regard to the central frequency  $4\pi c/\lambda_L$  (where  $\lambda_L = 1064 \text{ nm}$  is the exciting laser wavelength). The semiclassical spectra are denoted by dots and labeled by SC, whereas the quantum spectrum is plotted with lines (dash or solid) and labeled by QM; a discussion of the result uncertainties is within the text (Secs. IV A and IV B).

other, especially at low- and midrange frequencies. In fact, for the most prominent contributions the relative root mean square deviations between the SC and QM graphs equal 1.67%, 4.56%, and 16.24% ( $\lambda L = 01$ ) and 2.98%, 3.41%, and 16.05% ( $\lambda L = 03$ ) for  $\nu = 370.0, 600.0,$  and  $1500.0 \text{ cm}^{-1}$ , respectively (Fig. 5), which may serve as an additional measure of the stability of the two independent methods used. Since this is the peak frequency region of the translational spectra, which

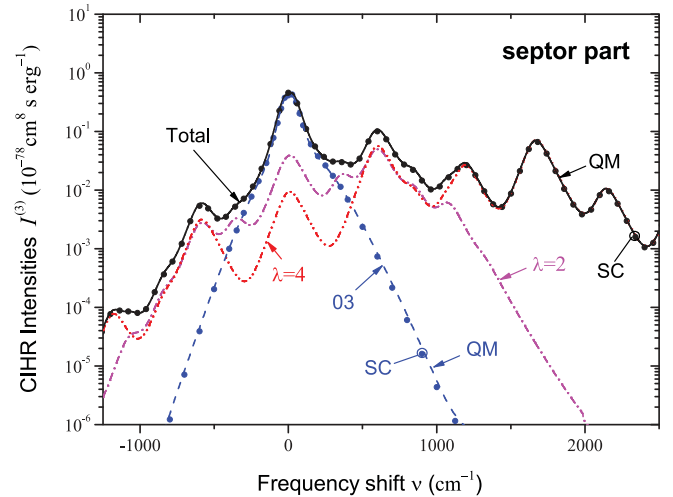


FIG. 4. (Color online) The CIHR binary polarized septor spectrum  $I_{\perp}$  (in  $\text{cm}^8 \text{ s erg}^{-1}$ ) of the H<sub>2</sub>-Ne pair at  $T = 295 \text{ K}$ , versus frequency shift ( $\nu$ , in  $\text{cm}^{-1}$ ) with regard to the central frequency  $4\pi c/\lambda_L$  (where  $\lambda_L = 1064 \text{ nm}$  is the exciting laser wavelength). The semiclassical spectra are denoted by dots and labeled by SC, whereas the quantum spectrum is plotted with lines (dash or solid) and labeled by QM; a discussion of the result uncertainties is within the text (Secs. IV A and IV B).

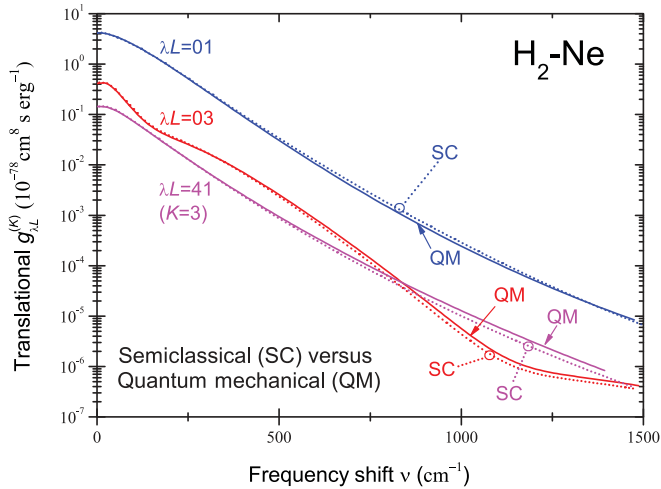


FIG. 5. (Color online) Comparison of the semiclassical and the quantum-mechanical profiles for the  $\lambda L = 01$  and  $03$  components of the transitional lines.  $\lambda L = 41$  (septor) contribution added to illustrate a higher-order case.

is mainly responsible for the intensities of the convoluted spectra, the discrepancies between the SC and QM graphs are hardly visible on a logarithmic scale. A similar remark can be made when using the formula of Birnbaum and Cohen (BC) [33,38], even if this analytical approach fails to reproduce well some translational line shapes, especially those for the  $\lambda L = 03$  septor component. As the BC formula depends only on three parameters, the semiclassical moments  $M_0$ ,  $M_1$ , and  $M_2$  associated with the symmetry-adapted components considered, it offers the possibility for the fast calculation of unfortunately unrefined spectral lines. What is more, as a result of the simplicity of this analytical model, it would be easy to fit any possible experimental profile to a theoretical spectrum directly deduced from the convolution of the rotational stick intensity set with the BC formulas. The latter are determined only by the values of the spectral moments, which therefore can be evaluated on the basis of that procedure for each value of  $\lambda$ . We have tested the feasibility of this fit by considering our own theoretical spectra  $I^{(1)}$  and  $I^{(3)}$  [Eq. (6)] as being *experimental* within the frequency range from  $-800$  to  $3000$   $\text{cm}^{-1}$ , in which the intensities are higher than the experimental threshold of  $10^{-82}$   $\text{cm}^8$   $\text{s erg}^{-1}$  reported in Sec. II. The fitted values of  $M_0$  obtained turned out to be in a satisfactory agreement with their theoretical values (within a few per cent). A similar convergence was found for  $M_1$  and  $M_2$ , except for the  $\lambda L = 03$  component, for which the BC profile differs significantly from the SC and QM cases, even at low frequencies (the disagreement reaching for  $M_0$ ,  $M_1$ , and  $M_2$  the levels of 1.5%, 53%, and 106%, respectively).

From the experimental point of view, any registered CIHR spectrum can be considered as a combination of the two,  $K = 1$  and  $K = 3$ , contributions:

$$I(\nu) = \chi^{(1)} I^{(1)}(\nu) + \chi^{(3)} I^{(3)}(\nu). \quad (8)$$

For example, for the experimental right-angle setup with the incident laser beam polarized perpendicularly to the scattering plane and the scattered signal detected at  $90^\circ$  without any

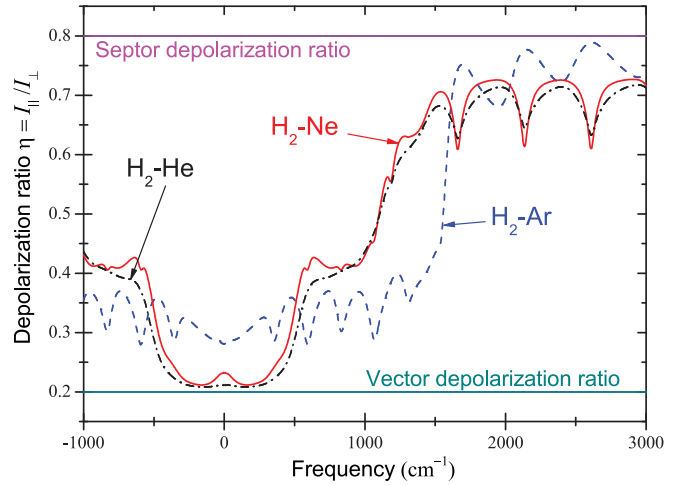


FIG. 6. (Color online) The depolarization ratios (DRs) of the CIHR spectra of  $\text{H}_2\text{-He}$ ,  $\text{H}_2\text{-Ne}$ , and  $\text{H}_2\text{-Ar}$  versus frequency shift. These DRs close to the vector-part value are equal to 0.2 in the low- and intermediate-frequency ranges and grow at the high-frequency Stokes side wings, approaching slowly the septor part value equal to 0.8.

analyzer, we have  $\chi^{(1)} = 2/9$  and  $\chi^{(3)} = 2/21$ , and thus we deal with the so-called *polarized* spectrum  $I_{\perp}(\nu)$  [33]. The corresponding *depolarized* spectrum  $I_{\parallel}(\nu)$  is obtained when the polarization of the incident laser beam is parallel to the scattering plane. In this case  $\chi^{(1)} = 2/45$  and  $\chi^{(3)} = 8/105$  [33]. The resulting depolarization ratio  $\eta(\nu) = I_{\parallel}/I_{\perp}$  is provided in Fig. 6 for  $\text{H}_2\text{-Ne}$  together with the depolarization ratios of the mixtures  $\text{H}_2\text{-He}$  and  $\text{H}_2\text{-Ar}$ . As can be checked in the latter figure, the vector contribution predominates for frequency shifts close to zero ( $|\nu| \leq 300$   $\text{cm}^{-1}$ ; 01 contribution). At high frequencies ( $\nu \geq 1300$   $\text{cm}^{-1}$ ), the septor part (mainly the 41 contribution) plays the leading role. Similar behavior can be noticed for the pairs  $\text{H}_2\text{-Ar}$  and  $\text{H}_2\text{-He}$ .

### B. CIHR versus $\Delta\beta(R)$ dependence

The data sets representing the hyperpolarizability tensor dependence on the intermolecular distance  $R$  contain the values of the property obtained for a relatively large distance range up to 14.0 bohr, with the lower limit reaching the points in rather close proximity to the colliding molecules—3.0 bohr. Consequently, it enables a careful estimation of the role played by the *close encounter* features of  $\Delta\beta(R)$ , which may be of great importance for the shape of the midrange translational spectral lines since some of the symmetry-adapted components of the hyperpolarizability exhibit characteristic nonmonotonic behavior for small intermolecular separations (Figs. 1 and 2). This kind of analysis, which is based on establishing a satisfactory convergence of the spectral profiles obtained by step-by-step gradual reduction of the lowest  $R$  limit of the computations, lets us conclude that for the  $\text{H}_2\text{-Ne}$  pair systems stable profiles are attained at the intermolecular separation of approximately 3.75 bohr for SA vector components and 3.80 bohr for the septor case—the distances are significantly lower than the potential collisional parameter  $\sigma$ , equal to 5.56 bohr for the system considered herein. Thus one can safely

assume that the short-range features of the hyperpolarizability with their nonmonotonic dependence really matter and the size of the molecules is of the essence, which is especially evident for the  $\lambda L = 03$  contribution (Fig. 2).

Similar results can be obtained for other molecular compounds of similar families studied previously—H<sub>2</sub>-He and H<sub>2</sub>-Ar [18,19], where the starting points of the convergence of the profiles are found to be equal to 3.55 and 3.35 bohr for the vector and septor contributions, respectively, in the

H<sub>2</sub>-He mixtures, whereas their counterparts for H<sub>2</sub>-Ar amount to around 4.50 (vector) and 4.55 bohr (septor).

#### ACKNOWLEDGMENTS

This paper was supported by the research project No. N N202 069939 sponsored by the government of the Republic of Poland. We thank Dr F. Lique for sending us numerical values for the H<sub>2</sub>-Ne potential.

- 
- [1] G. Herzberg, *Astrophys. J.* **115**, 337 (1952).
- [2] J. E. Dove, A. C. M. Rusk, P. H. Cribb, and P. G. Martin, *Astrophys. J.* **318**, 379 (1987).
- [3] M. Abel, L. Frommhold, X. Li, and K. L. C. Hunt, *J. Phys. Chem.* (accepted).
- [4] L. Schlapbach and A. Zuetzel, *Nature (London)* **414**, 353 (2001).
- [5] M. K. Kostov, H. Cheng, R. M. Herman, M. W. Cole, and J. C. Lewis, *J. Chem. Phys.* **116**, 1720 (2002).
- [6] A. M. Dunker and R. G. Gordon, *J. Chem. Phys.* **68**, 700 (1978).
- [7] P. Barletta, *Eur. Phys. J. D* **53**, 33 (2009).
- [8] P. Barletta, J. Tennyson, and P. F. Barker, *Phys. Rev. A* **78**, 052707 (2008).
- [9] M. Faubel, F. A. Gianturco, F. Ragnetti, L. Y. Rusin, F. Sondermann, U. Tappe, and J. P. Toennies, *J. Chem. Phys.* **101**, 8800 (1994).
- [10] F. Lique, *Chem. Phys. Lett.* **471**, 54 (2009).
- [11] R. D. Pyatt and D. P. Shelton, *J. Chem. Phys.* **114**, 9938 (2001).
- [12] G. Boudebs and K. Fedus, *J. Appl. Phys.* **105**, 103106 (2009).
- [13] J. Dawesa and M. Sceats, *Opt. Commun.* **65**, 275 (1988).
- [14] W. Głaz and T. Bancewicz, *J. Chem. Phys.* **118**, 6264 (2003).
- [15] W. Głaz, T. Bancewicz, and J.-L. Godet, *J. Chem. Phys.* **122**, 224323 (2005).
- [16] W. Głaz, T. Bancewicz, J.-L. Godet, G. Maroulis, and A. Haskopoulos, *Phys. Rev. A* **73**, 042708 (2006).
- [17] G. Maroulis, A. Haskopoulos, W. Głaz, T. Bancewicz, and J.-L. Godet, *Chem. Phys. Lett.* **428**, 28 (2006).
- [18] T. Bancewicz and G. Maroulis, *Phys. Rev.* **79**, 042704 (2009).
- [19] J.-L. Godet, T. Bancewicz, W. Głaz, G. Maroulis, and A. Haskopoulos, *J. Chem. Phys.* **131**, 204305 (2009).
- [20] X. Li, C. Ahuja, J. F. Harrison, and K. L. C. Hunt, *J. Chem. Phys.* **126**, 214302 (2007).
- [21] S. F. Boys and F. Bernardi, *Mol. Phys.* **19**, 55 (1970).
- [22] M. J. Frisch, G. W. Trucks, H. B. Schlegel *et al.*, GAUSSIAN 03, Revision D.01 (Gaussian, Inc., Wallingford, CT., 2004).
- [23] T. Helgaker, P. Jørgensen, and J. Olsen, *Molecular Electronic-Structure Theory* (Wiley, Chichester, 2000).
- [24] G. Maroulis, *J. Phys. Chem. A* **104**, 4772 (2000).
- [25] G. Maroulis and D. M. Bishop, *Chem. Phys. Lett.* **128**, 462 (1986).
- [26] J. Stiehler and J. Hinze, *J. Phys. B* **28**, 4055 (1995).
- [27] A. Haskopoulos, G. Maroulis, and T. Bancewicz (unpublished).
- [28] P. D. Maker, *Phys. Rev. A* **1**, 923 (1970).
- [29] W. H. Press, S. A. Teukolsky, W. T. Vetterling, and B. P. Flanery, *Numerical Recipes* (Cambridge University Press, Cambridge, 1996).
- [30] L. Frommhold, *Collision-induced Absorption in Gases* (Cambridge University Press, Cambridge, 1993).
- [31] X. Li, K. L. C. Hunt, J. Pipin, and D. M. Bishop, *J. Chem. Phys.* **105**, 10954 (1996).
- [32] T. Bancewicz, *J. Chem. Phys.* **111**, 7440 (1999).
- [33] T. Bancewicz, W. Głaz, J.-L. Godet, and G. Maroulis, *J. Chem. Phys.* **129**, 124306 (2008).
- [34] W. Głaz, J. Yang, J. D. Poll, and C. G. Gray, *Chem. Phys. Lett.* **218**, 183 (1994).
- [35] L. Frommhold, *Adv. Chem. Phys.* **46**, 1 (1981).
- [36] W. Głaz and G. C. Tabisz, *Can. J. Phys.* **79**, 801 (2001).
- [37] H. Posch, *Mol. Phys.* **46**, 1213 (1982).
- [38] G. Birnbaum and E. R. Cohen, *Can. J. Phys.* **54**, 593 (1976).